Available online at www.sciencedirect.com

ScienceDirect

Ceramics International 39 (2013) 9471–9481

CERAMICS INTERNATIONAL

www.elsevier.com/locate/ceramint

Unraveling the mechanical and tribological properties of a novel Ti_5Si_3/TiC nanocomposite coating synthesized by a double glow discharge plasma technique

Jiang Xu[a], Linlin Liu[a], Lei Jiang[b,*], Paul Munroe[c], Zong-Han Xie[d]

[a]*Department of Material Science and Engineering, Nanjing University of Aeronautics and Astronautics, 29 Yudao Street, Nanjing 210016, PR China*
[b]*School of Environmental Engineering, Wuhan Textile University, Wuhan 430073, PR China*
[c]*School of Materials Science and Engineering, University of New South Wales, NSW 2052, Australia*
[d]*School of Mechanical Engineering, University of Adelaide, SA 5005, Australia*

Received 15 April 2013; received in revised form 1 May 2013; accepted 3 May 2013
Available online 30 May 2013

Abstract

A novel Ti_5Si_3/TiC nanocomposite coating has been successfully prepared on a Ti–6Al–4V substrate by a double cathode glow discharge technique to address its poor tribological properties. The microstructural features of the Ti_5Si_3/TiC nanocomposite coating were characterized by X-ray diffraction (XRD), scanning electron microscopy (SEM) and transmission electron microscopy (TEM). The nanocomposite coating consisted of cauliflower-like Ti_5Si_3 grains with an average grain size of ~15 nm and TiC nanoparticles having an average grain size of ~15 nm distributed at its boundaries. The mechanical and tribological properties of the Ti_5Si_3/TiC nanocomposite coating were compared with those of a monolithic Ti_5Si_3 nanocrystalline coating. The results clearly showed that the Ti_5Si_3/TiC nanocomposite coating exhibited a unique combination of higher fracture toughness and hardness as compared to the monolithic Ti_5Si_3 nanocrystalline coating, which thus exerted a positive effect on its wear resistance.

Keywords: C. Wear resistance; C. Mechanical properties; C. Friction; D. Silicides

1. Introduction

Titanium alloys are widely used in aerospace, chemical, medical and marine industries as key structural components due to their excellent combination of high specific strength, good ductility, notable resistance to fatigue and corrosion and superior biocompatibility [1,2]. However, titanium alloys have poor tribological properties, manifested by a high and unstable friction coefficient, low adhesive, abrasive and fretting wear resistance [3], posing a clear bottleneck that limits their widespread engineering applications, especially as sliding contact components [4,5]. The wear process of materials is a gradual accumulation of damage originating from the constant, dynamic interactions of contacting surfaces that are subjected to mechanical stresses. As such, it is governed by the microstructure and composition of the near-surface region in the material. With this in mind, surface modification is considered to be one of the most efficient approaches to improve the tribological properties of titanium alloys, and thus may expand their range of applications into much harsher working environments. For this reason, a variety of surface engineering technologies, including laser surface treatment [6], plasma immersion ion implantation (PIII) [7], chemical vapor deposition (CVD) [8,9] and physical vapor deposition (PVD) [10,11], have been developed in an attempt to significantly enhance the surface properties of titanium alloys. In our previous studies [12,13], a double glow discharge plasma technique was used and proved to be a novel and feasible means of fabricating hard and wear resistant coatings on titanium alloys.

Ti_5Si_3 has received much attention because of its potential advantages over other silicides, such as high melting point

---

*Corresponding author. Tel.: +86 2787611623.
E-mail address: jiangqiang51@sina.cn (L. Jiang).

0272-8842/$ - see front matter © 2013 Elsevier Ltd and Techna Group S.r.l. All rights reserved.
http://dx.doi.org/10.1016/j.ceramint.2013.05.065

(2130 °C), relatively low density (4.32 g/cm^{-3}), excellent oxidation and creep resistance, and is thus an attractive candidate for high-temperature applications [14,15]. In addition, owing to its high hardness and chemical stability stemming from covalent-dominated atomic bonds in its crystal structure, monolithic Ti_5Si_3 has been recognized as a new generation of wear resistant coating material for surface protection of moving components working under aggressive environments. However, as in the case of many intermetallic compounds, a major limitation for the use of this material is its poor fracture toughness, due mainly to its complex hexagonal crystal structure, with low symmetry and strong covalent bonding, which increases the Peierls stress [16]. A number of attempts have been made to overcome this limitation. Routes commonly utilized include the addition of a second phase to form composites and the refinement of the grain size to the nanoscale [17,18]. One prominent example of Ti_5Si_3-based composites is fabricated by the addition of TiC to Ti_5Si_3 to improve the mechanical properties of monolithic Ti_5Si_3. TiC is an appropriate strengthening phase for the Ti_5Si_3 matrix due to a good match between the thermal expansion coefficient of Ti_5Si_3 and TiC (7.7×10^{-6} °C^{-1} for TiC and 9.7×10^{-6} °C^{-1} for Ti_5Si_3) [19]. Wang et al. [20] found that fracture toughness of a TiC/Ti_5Si_3 composite fabricated by spark plasma sintering was more than 50% higher than monolithic Ti_5Si_3. So far, most investigations have been focused on the mechanical properties (i.e., fracture toughness) of bulk Ti_5Si_3-based composites. However, there has been little effort devoted to study of their mechanical properties and wear behavior in these coatings, which is critical to their intended engineering applications.

In the current work, a novel Ti_5Si_3/TiC nanocomposite coating was deposited on to a Ti–6Al–4V substrate for the first time by a double glow discharge plasma technique. The composition and microstructure of the as-deposited coatings were first characterized by X-ray diffraction (XRD), scanning electron microscopy (SEM) and transmission electron microscopy (TEM). Then, the mechanical properties, adhesion strength, and wear resistance of the newly-developed coating were explored, with an effort to gain better understanding of the relationship between the mechanical and tribological properties and microstructure of the Ti_5Si_3/TiC nanocomposite coating.

2. Experimental method

2.1. Specimen preparation

The substrate material used was a Ti–6Al–4V alloy with a diameter of 40 mm and a thickness of 3 mm. The nominal composition in wt% was: Al, 6.04; V, 4.03; Fe, 0.3; C, 0.1; H, 0.015; N, 0.05; O, 0.15; and the balance, Ti. Before deposition, the Ti–6Al–4V substrates were polished using silicon carbide abrasive paper of 2400 grit and then cleaned in pure alcohol using an ultrasonic cleaner. The monolithic Ti_5Si_3 nanocrystalline coating and Ti_5Si_3/TiC nanocomposite coating were deposited onto the substrates by a double cathode glow discharge apparatus using two targets with different stoichiometric ratios (i.e., $Ti_{50}Si_{50}$ and $Ti_{40}Si_{40}C_{20}$), respectively. The sputtering targets were fabricated from ball-milled Ti (-300 mesh, $>99.9\%$ purity), Si (-200 mesh, $>99.5\%$ purity), and C powders (graphite, -500mesh, $>99.9\%$ purity) by employing cold compaction under a pressure of 600 MPa. In the deposition process, one cathode is used as the target composed of the desired sputtering materials, and the other cathode is the substrate material. When two different voltages are applied to the two cathodes, glow discharge occurs, as described elsewhere [21]. The glow discharge sputtering conditions are as follows: base pressure, 5×10^{-3} Pa; working pressure, 35 Pa; target electrode bias voltage with direct current, −950 V; substrate bias voltage with impulse current, −350 V; substrate temperature, 950°C; target-substrate distance, 10 mm and treatment time 3 h. The reasons for such a difference in the composition of the targets and the deposited coatings are that the composition of the as-deposited coatings is related not only to the composition of target materials, but also the sputtering yields of the various elements in the target materials. Furthermore, the diffusion of different alloying elements at the interface between the as-deposited coating and substrate also affects the composition of the coating.

2.2. Microstructure characterization

The phase compositions of the as-deposited films were studied by X-ray diffractometry (XRD, D8ADVANCE with Cu Kα radiation) operating at 35 kV and 40 mA. X-ray spectra were collected in the 2θ range from 20° to 90° with a scan rate of 0.05°/s. The cross-section of specimens was prepared and etched with the use of Kroll's reagent (10 ml HNO_3, 4 ml HF and 86 ml distilled water) for 20–30 s. The cross-sectional morphology and chemical composition of the as-deposited coatings were examined by scanning electron microscopy (SEM, Quanta 200, FEI Company) equipped with an energy-dispersive X-ray spectrometer (EDS, EDAX Inc.). Transmission electron microscopy (TEM) and high-resolution transmission electron microscopy (HRTEM)

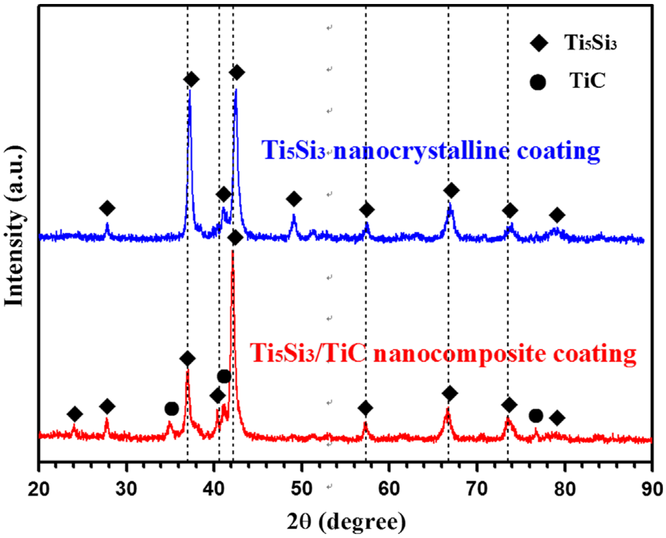

Fig. 1. XRD patterns of the as-deposited Ti_5Si_3 nanocrystalline coating and Ti_5Si_3/TiC nanocomposite coating.

images were taken using a JEOL JEM-2010 at an accelerating voltage of 200 kV. Plan-view samples for TEM observation were prepared using a single-jet electrochemical polishing technique from the untreated side of the substrate.

2.3. Nanoindentation and scratch tests

Nanoindentation tests were conducted on all the as-deposited coatings using a nanoindentation tester (NHT) equipped with a Berkovich diamond tip. This system, developed by CSEM Instruments, comprises two distinct components: a measuring head for performing nanoindentation and an optical microscope for selecting a specific sample site prior to indentation, and for checking the location of the imprint after indentation. The system has load and displacement resolutions of 10 μN and 1 nm, respectively. Fused silica was used as a standard sample for the initial tip calibration. The indentation was performed by driving the indenter at a constant loading rate of 40 mN/min into the material surface with a maximum applied load of 20 mN. Hardness and the elastic modulus were evaluated using the Oliver–Pharr method [22] based on the load–displacement data obtained during the indentation tests. Each hardness and elastic modulus data were derived from the load–displacement curves of at least five indentations to ensure repeatability of the experimental data. Adhesion strength of the as-deposited coating was evaluated by a commercial scratch tester (WS-97), equipped with an acoustic emission (AE) detector. The scratch tests were performed by drawing a 200 μm radius Rockwell C diamond indenter across the coating surfaces under a normal load increasing linearly from 0 to 100 N. The loading rate was set at 20 N/min and a scratch speed was 1 mm/min. An AE sensor was attached near the diamond indenter tip to detect the acoustic signals emitted from the coating failure. The minimum load at which a sudden increase in the intensity of the acoustic signals occurs is defined as the critical load (L_c) that represents the coating adhesion strength.

2.4. Wear tests

Dry wear tests were performed using a HT-500 tribometer with a ball-on-disk configuration at room temperature. In this

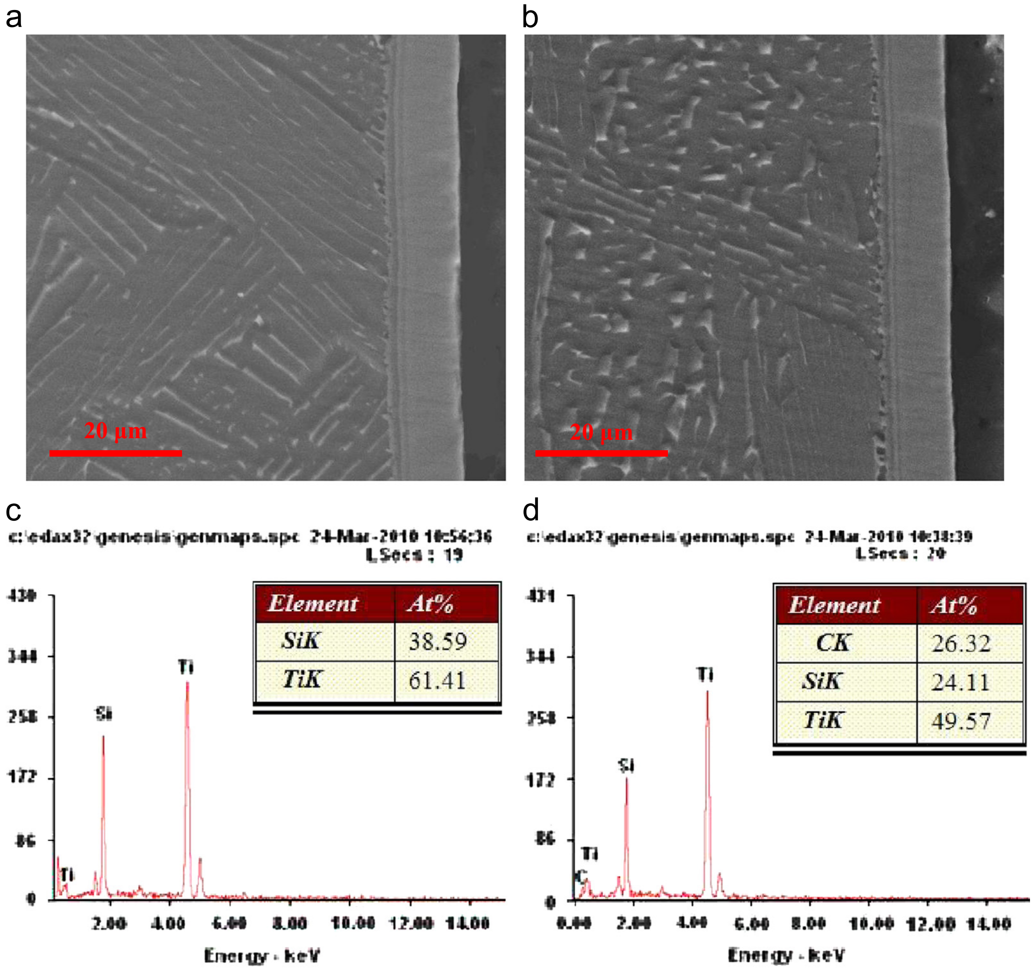

Fig. 2. Cross-sectional SEM morphologies and energy dispersive X-ray (EDX) spectra of the as-deposited Ti_5Si_3 nanocrystalline coating (a, c) and Ti_5Si_3/TiC nanocomposite coating (b, d).

work, the upper balls, 3 mm in diameter, were made of ZrO_2 with a hardness of 1300 H_V and a surface roughness (R_a) of 0.35 μm, and the lower disc samples ($10 \times 10 \times 3$ mm^3) were machined from both uncoated and coated Ti–6Al–4V. The surfaces of the specimens were ground and polished prior to the wear test. During the wear test, the ceramic ball tip was sliding on the specimen along a circle with 6 mm diameter at a sliding velocity of 0.22 ms^{-1} under the applied normal loads of 3.8 N and 4.8 N. The friction coefficient was continuously recorded using a Dell PC connected to the ball-on-disc test rig. The total sliding distance for the tests was 792 m. The profile of the wear tracks on the specimens was measured by a profilometer (Micro-XAMTM, ADE phase-shift company) to determine the worn volume. The specific wear rate of the films, W, was calculated:

$$W = \frac{V}{FS} \tag{1}$$

where V is the volume of worn material, F is normal load and S is the sliding distance.

3. Results and discussion

3.1. Microstructures and phase analysis

X-ray diffraction patterns taken from the as-deposited Ti_5Si_3 nanocrystalline coating and Ti_5Si_3/TiC nanocomposite coating are shown in Fig. 1. The diffraction peaks obtained from the Ti_5Si_3 nanocrystalline coating can be indexed to be consistent with hexagonal $D8_8$-structured Ti_5Si_3. Compared with the powder diffraction file data (No. 29-1362) for Ti_5Si_3 (represented by vertical lines), the peak positions for Ti_5Si_3 phase shift to higher angles, which indicates the presence of residual tensile stresses in the monolithic Ti_5Si_3 nanocrystalline coating. For the Ti_5Si_3/TiC nanocomposite coating, in addition to Ti_5Si_3 that is identified as the dominant phase, minor amounts of TiC are also detected. Moreover, it can be seen that the diffraction peak positions of Ti_5Si_3 in the Ti_5Si_3/TiC nanocomposite coating are strongly consistent with those of the powder diffraction file data, which is related to a fraction of the carbon atoms becoming dissolved in Ti_5Si_3 to occupy

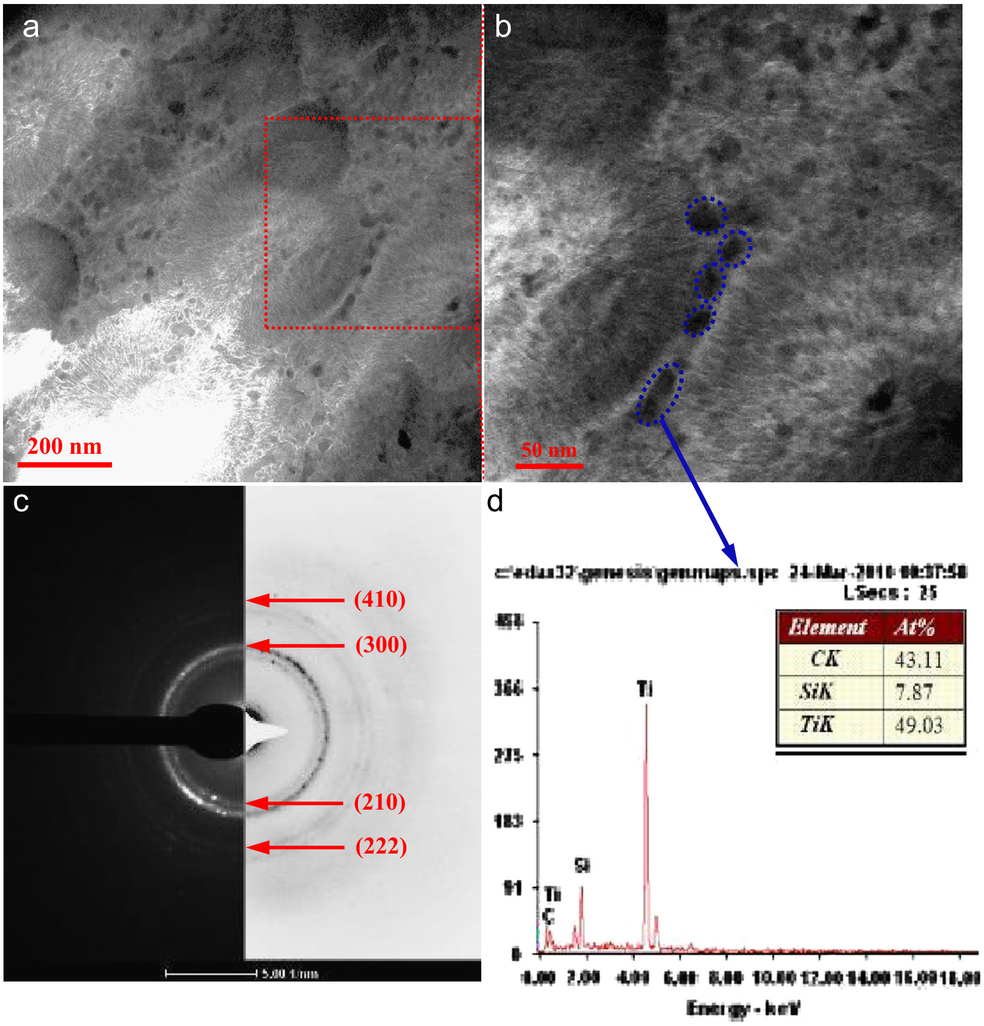

Fig. 3. (a) TEM bright-field image of the as-deposited Ti_5Si_3/TiC nanocomposite coating; (b) high magnification image marked in (a); (c) selected area electron diffraction (SEAD) pattern of the cauliflower-like structure in (b); and (d) energy dispersive X-ray (EDX) spectrum of the particles circled by blue dotted lines in (b).

interstitial sites, thus resulting in a reduction in the residual tensile stresses in the coating.

Fig. 2 shows the typical cross-sectional SEM images and the corresponding EDS spectra of both the as-deposited Ti_5Si_3 nanocrystalline coating and Ti_5Si_3/TiC nanocomposite coating. As shown in Fig. 2(a) and (b), there are no visible defects or cracks over the cross-section of the two as-deposited coatings, and interface between the coating and the substrate is continuous, indicating that the two as-deposited coatings are tightly adhered to the substrate. The microstructure of the two as-deposited coatings can be classified into two layers, namely, the ~10 μm thick outer deposition layer and an inner diffusion layer with a thickness of ~2 μm. EDS area analysis indicates that the outer layer of the Ti_5Si_3 nanocrystalline coating has the Si/Ti atomic ratio (38.59:61.41) approaching the theoretical proportion value of 0.6 in Ti_5Si_3, indicating that the outer layer is composed of single phase Ti_5Si_3; for the Ti_5Si_3/TiC nanocomposite coating, the outer layer is composed of the Ti, Si and C, and combined when with the XRD and EDS results, it may be inferred that the microstructure of outer layer consists of both Ti_5Si_3 and TiC phases. Fig. 3(a) shows typical TEM plan-view observations of the outer layer obtained from the Ti_5Si_3/TiC nanocomposite coating. It is clear that the microstructure of outer layer is characterized by a cauliflower-like structure with some irregular nanoparticles (marked by blue dotted lines) distributed over its boundaries. A very similar microstructure feature is also observed for the outer layer of Ti_5Si_3 nanocrystalline coating, as described in our previous work [23]. A high-resolution image (Fig. 3(b)) from the selected section in Fig. 3(a) reveals that the cauliflower-like architecture is an assembly of nanocrystallites with an average grain size of ~15 nm. A selected-area electron diffraction (SAED) pattern (Fig. 3(c)) obtained from the cauliflower-like architecture indicates that diffraction rings can be indexed to the (210), (300), (222) and (410) lattice planes of hexagonal $D8_8$-structured Ti_5Si_3. Because the size of the irregular nanoparticles distributed among the boundaries of the cauliflower-like architecture is too small to be discerned in the SAED pattern, those nanoparticles are further analyzed by EDS microanalyses (Fig. 3(d)). The results of EDS analysis indicate that these irregular nanoparticles contain a significant amount of both Ti and C, with a minor amount of Si, suggesting that these nanoparticles may be TiC. The detection of silicon in this region is likely due to the fact that the size of nanoparticles is smaller than that of the focused electron beam used in EDS mode.

3.2. Mechanical properties

3.2.1. Nanoindentation tests.

Typical load–displacement (*p*–*h*) curves obtained from instrumented nanoindentation for the Ti_5Si_3/TiC nanocomposite coating, the Ti_5Si_3 nanocrystalline coating and the untreated Ti–6Al–4V substrate indented with a maximum load of 20 mN are presented in Fig. 4(*a*). The smooth curves on the loading part of both coatings indicate that no fracture or delamination of the coatings occurred during nanoindentation testing. Since the largest indentation depth of the diamond indenter penetration into the two as-deposited coatings is lower than 10% of the coating thickness, the total deformation is confined within the coating and any substrate effects are negligible. Fig. 4(b) shows hardness (*H*) and Young's modulus (*E*) values calculated using the Oliver–Pharr method based on the load displacement data obtained from the two as-deposited coatings and the untreated Ti–6Al–4V substrate. The hardness values of the Ti_5Si_3/TiC

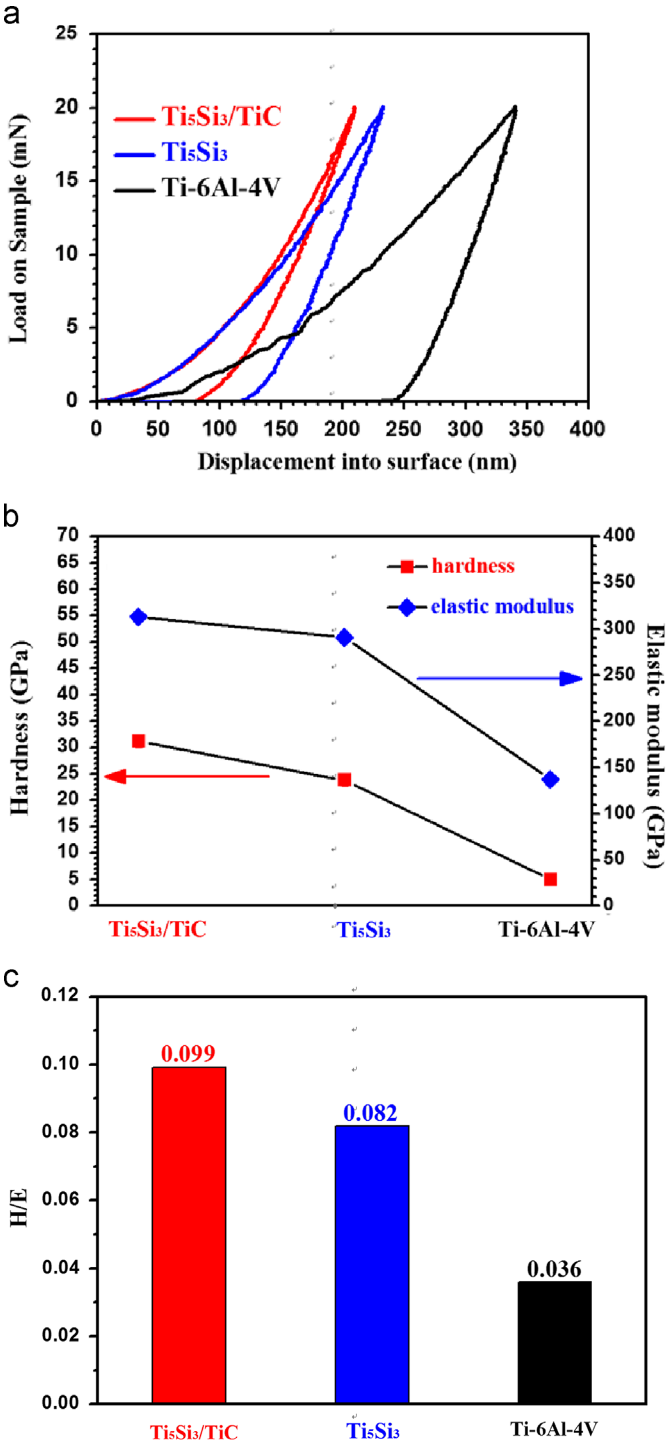

Fig. 4. Load–displacement curves (a), hardness and elastic modulus (b) and and H/E (c) of the two as-deposited coatings and the uncoated Ti–6Al–4V alloy.

nanocomposite coating and the Ti_5Si_3 nanocrystalline coating were determined to be 31.1 ± 1.2 GPa and 23.8 ± 1.1 GPa, respectively, both of which are significantly greater than that of coarse grained Ti_5Si_3 reported in the literature ($H = 11.3 \pm 0.54$ GPa) [24]. Similar findings were also observed in our previous work [25]. Moreover, the two as-deposited coatings show the close resemblance of their elastic properties (the Young's modulus of theTi_5Si_3/TiC nanocomposite coating is 313.7 ± 4 GPa and for the Ti_5Si_3 nanocrystalline coating, Young's modulus is 291.3 ± 6 GPa). This is also demonstrated by the unloading parts of both coatings which are very similar. Usually the hardness of a material is determined by its intrinsic resistance to plastic deformation, i.e., depending on the amount of obstacles to plastic deformation provided by a material. For nanocrystalline metals and alloys, strength decreases once grain sizes are below a certain grain size (~20 nm), where an "inverse Hall–Petch-type" relationship is observed both by experimental research [26] and atomistic simulations [27]. The reason for this behavior is attributed to crossover in the prevailing mechanism from dislocation-mediated deformation to grain boundary-mediated deformation below the critical grain size [28]. Nevertheless, for the covalent compound, its hardness is closely related to the nature of interatomic bonding and its response to strain at the atomistic level. As the grain size of the covalent compound is reduced to the nanoscale, the conduction/valence band edging generally shifts to a higher energy relative to the bulk material and increases the band gap, leading to an enhancement in hardness. Gao [29] and Tse [30] observed in recent experiments that the hardness of nanocrystalline covalent solids, such as BC_2N or diamond, increases noticeably with decreasing the grain sizes to less than 10 nm, which may be interpreted as a quantum confinement effect. Furthermore, the presence of TiC within the nanocomposite coating, acting as a physical barrier for intergranular shear sliding, further improves the coating hardness by means of an extrinsic strengthening mechanism. Some researchers have proposed that the ratio of hardness and elastic modulus (H/E) is widely quoted as a valuable measure in determining the limit of elastic behavior in a surface contact, and as a ranking parameter for predicting wear resistance of coating [31]. As shown in Fig. 4(c), the H/E ratio of the Ti_5Si_3/TiC nanocomposite coating is higher than that of the Ti_5Si_3 nanocrystalline coating, indicative of a potential increase in wear resistance of the Ti_5Si_3-based coating by forming a composite with TiC.

3.2.2. Indentation fracture toughness.

In order to evaluate the contact-damage resistance of the two as-deposited coatings, the indentation fracture toughness was assessed using different applied loads ranging from 100 to 1000 g with a Vickers indenter. Fig. 5 shows optical micrographs of Vickers indentations on both the Ti_5Si_3 nanocrystalline coating and Ti_5Si_3/TiC nanocomposite coating. When the applied load increases to 500 g, the radial cracks emanating from the indentation corners are observed for the Ti_5Si_3 nanocrystalline coating, whereas there is no evidence of cracking at the indentation corners for the Ti_5Si_3/TiC

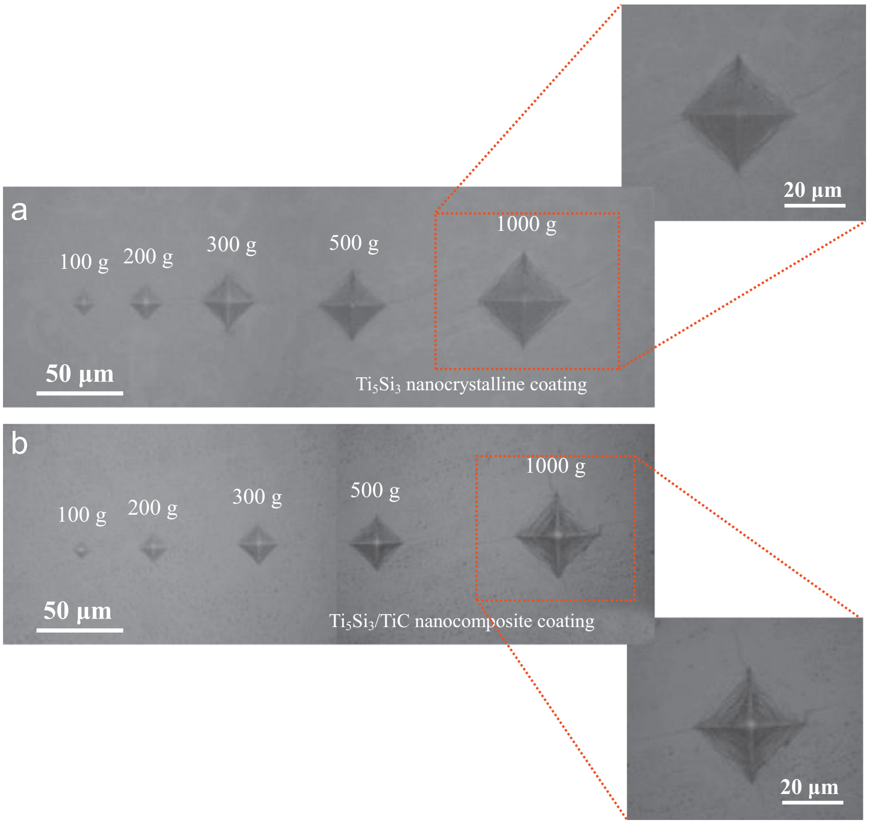

Fig. 5. Optical micrographs of Vickers indentations on the Ti_5Si_3 nanocrystalline coating (a) and the Ti_5Si_3/TiC nanocomposite coating (b).

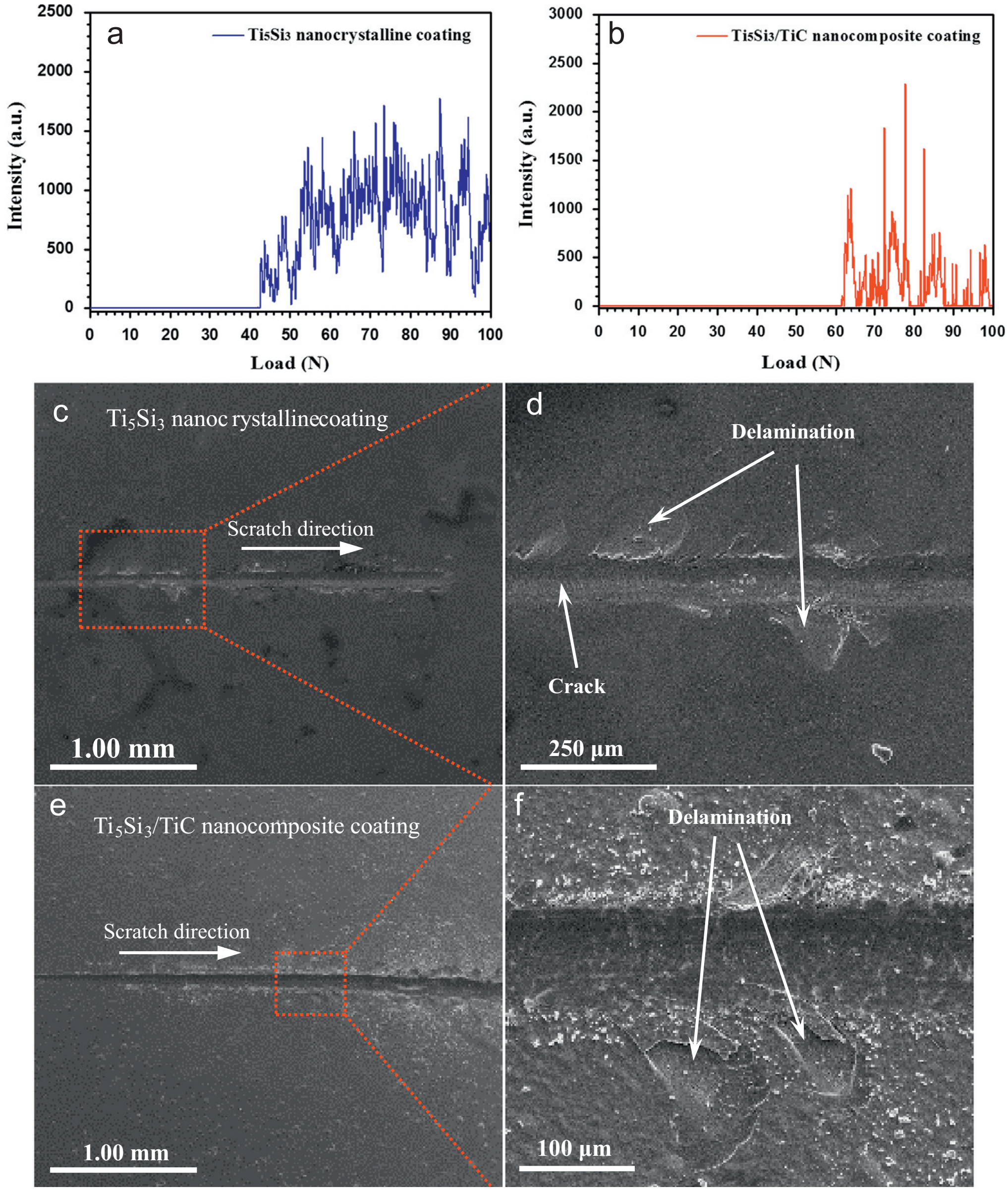

Fig. 6. Representative curves of acoustic emission vs. normal load for the Ti_5Si_3 nanocrystalline coating (a) and the Ti_5Si_3/TiC nanocomposite coating (b). SEM micrographs of scratch of the Ti_5Si_3 nanocrystalline coating (c), (d) high magnifications of a selected area in (c). SEM micrographs of scratch of the Ti_5Si_3/TiC nanocomposite coating (e), (f) high magnifications of a selected area in (e).

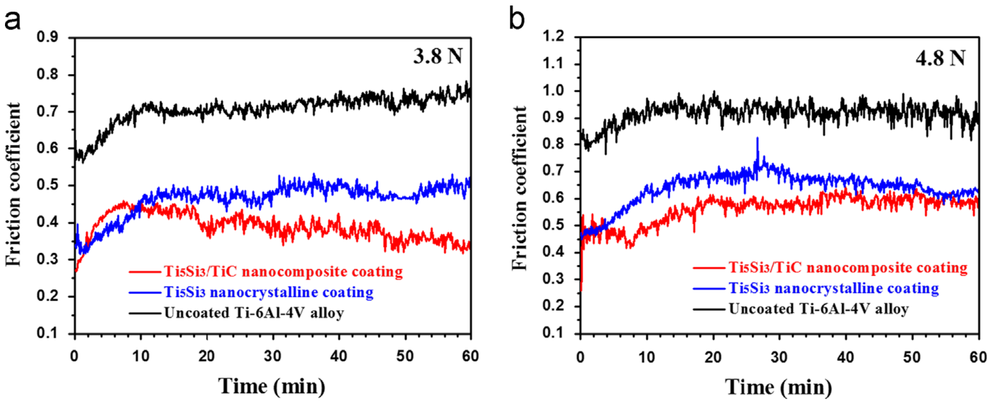

Fig. 7. Friction coefficient vs. sliding time curves for the two as-deposited coatings and uncoated Ti–6Al–4V alloy sliding against ZrO_2 ceramic ball under the normal loads of 3.8 (a) and 4.8 N (b).

nanocomposite coating until the indentation load reaches 1000 g. This implies that the Ti_5Si_3/TiC nanocomposite coating shows that greater energy is required to generate a crack or a higher threshold value for crack formation as compared to the Ti_5Si_3 nanocrystalline coating. The indentation fracture toughness (K_{IC}) values for the two coatings can be roughly evaluated by measuring the lengths of radial cracks propagating from the corners of the Vickers indentations according to the following equation [32]:

$$K_{\mathrm{IC}} = 0.204\left(\frac{c}{a}\right)^{-3/2} H_{\mathrm{v}} a^{1/2} \tag{2}$$

where c is the trace length of the crack measured from the center of the indentation, a is one-half of the average length of the two indent diagonals and H_{v} is the hardness. The calculated fracture toughness values for the Ti_5Si_3 nanocrystalline coating and Ti_5Si_3/TiC nanocomposite coating are about 3.7 and 11.5 MPa m$^{1/2}$, respectively. This result shows that the fracture toughness of Ti_5Si_3 is increased by a factor of three through incorporation of TiC. Experimental data obtained using the same model reported in the literatures indicate that the indentation fracture toughness values for the coarse grained monolithic Ti_5Si_3 and Ti_5Si_3-35 vol% TiC composite are 2.5 MPa m$^{1/2}$ and 4.2 MPa m$^{1/2}$ [20], respectively. Thus, a reduction in grain size to the nanometer scale is helpful in improving the indentation fracture toughness for both a monolithic Ti_5Si_3 and a Ti_5Si_3-based composite. The magnified images of the radial crack paths at the applied load of 1000 g show that the Ti_5Si_3/TiC nanocomposite coating presents a greater degree of tortuosity, indicative of crack deflection as an important toughening mechanism in the enhanced fracture toughness.

Furthermore, due to the large difference between the thermal expansion coefficients along the crystallographic a (5.98×10^{-6} K^{-1}) and c (16.64×10^{-6} K^{-1}) directions, monolithic Ti_5Si_3 is extremely anisotropic in its thermal expansion (CTE(c)/CTE(a) ratio of 2.8) [33], which leads to the formation of significant residual thermal stresses inside the grains of polycrystalline Ti_5Si_3 during cooling from the processing temperature, and even gives rise to microcracking [34]. These residual thermal stresses have negative effect on the mechanical properties of Ti_5Si_3, including poor room-temperature hardness and fracture toughness [35,36]. Previous studies have demonstrated that both refining the grain size and suitable alloying additions can reduce the adverse impact of the anisotropy of the coefficient of thermal expansion significantly. Thom et al. [37] have measured a critical grain size of 4 μm for Ti_5Si_3, above which the residual stresses are large enough to cause microcracking due to the CTE anisotropy. Fu et al. [38] suggested that the high thermal expansion anisotropy of Ti_5Si_3 originates from a chain of face-shared octahedral of titanium atoms in the c-direction, which exhibits a high anharmonicity and causes a high thermal expansion in the c-direction. Alloying Ti_5Si_3 with interstitial atoms, such as carbon, nitrogen and oxygen, lowers the CTE(c) markedly due to replacement of weak metallic bonds associated with the octahedral chain with stronger titanium–interstitial covalent bonds. Williams et al. reported [39] that carbon addition reduces the CTE anisotropy for pure Ti_5Si_3 from ~3 to ~1.9. Therefore, the Ti_5Si_3/TiC nanocomposite coating exhibits a lower residual stress by a beneficial combination of nanoscale grains and carbon doping effects, which also contributes to the enhancement in its fracture toughness.

3.2.3. Scratch test

Scratch resistance is a good indicator of not only adhesion strength between the coating and the substrate, but also the load bearing capacity, fracture toughness and abradability of a coating [40–42]. The acoustic emission curves are plotted as a function of the normal load in Fig. 6(a)–(b), and the corresponding SEM images of the scratch track are displayed in Fig. 6(c)–(f). No acoustic emission signals are detected at the early stage of scratching, and subsequently continuous acoustic emission peaks emerged after the applied load was greater than a critical load. The critical loads for the Ti_5Si_3/TiC nanocomposite coating and the Ti_5Si_3 nanocrystalline coating are 62 and 42 N, respectively. As a general rule, a critical load of above 30 N measured with a Rockwell C diamond tip in scratch testing is believed to be sufficient for sliding contact applications [40]. Thus, the two as-deposited coatings are likely to be suitable for wear applications involving high loads. As shown in Fig. 6(c)–(f), at an applied load less than the critical load, the scratch tracks appear to exhibit smooth morphologies without visible delamination or microcracking. As the applied loads reach critical loads, the scratch tracks clearly show microscopic failures within the coatings, characterized by the parallel cracks at the bottom of the scratch tracks and a large area of delamination at the edge of the scratch tracks. From SEM morphological observations of the scratch tracks, it can be seen that the Ti_5Si_3 nanocrystalline coating suffers more severe delamination and shows a higher crack density than the Ti_5Si_3/TiC nanocomposite coating, which is in accordance with the higher intensity of the acoustic emission peak. It is worthwhile to note that scratch resistance is a good indicator of not only adhesion strength between the coating and the substrate, but also the load bearing capacity and abradability of a coating [41–43]. Therefore, the introduction of TiC is beneficial not only to the enhancement of adhesion strength, but also to the improvement of these properties.

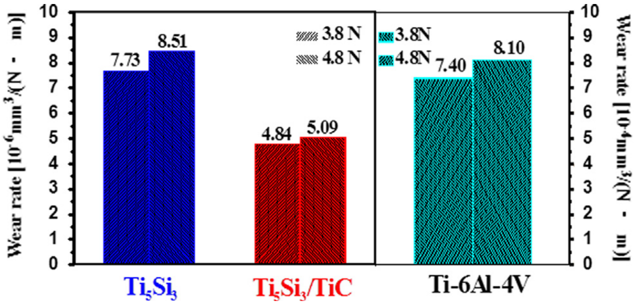

Fig. 8. Specific wear rates of the two as-deposited nanocrystalline coatings and reference Ti–6Al–4V alloy sliding against ZrO_2 ceramic ball under the normal loads of 3.8 and 4.8 N.

3.3. Friction and wear experiments

The ball-on-disc configuration, which has been used to simulate wear process that occurs in dynamically loaded components such as bearings, gears and crankshafts, was applied to evaluate the wear resistance of the specimens. Fig. 7 shows the change in friction coefficient as a function of sliding time for the two as-deposited coatings and the uncoated Ti–6Al–4V substrate sliding against ZrO_2 ceramic balls under the normal loads of 3.8 and 4.8 N. As can be seen in Fig. 7, all of the friction coefficient curves follow a similar tendency, where the friction coefficient increases rapidly in the initial

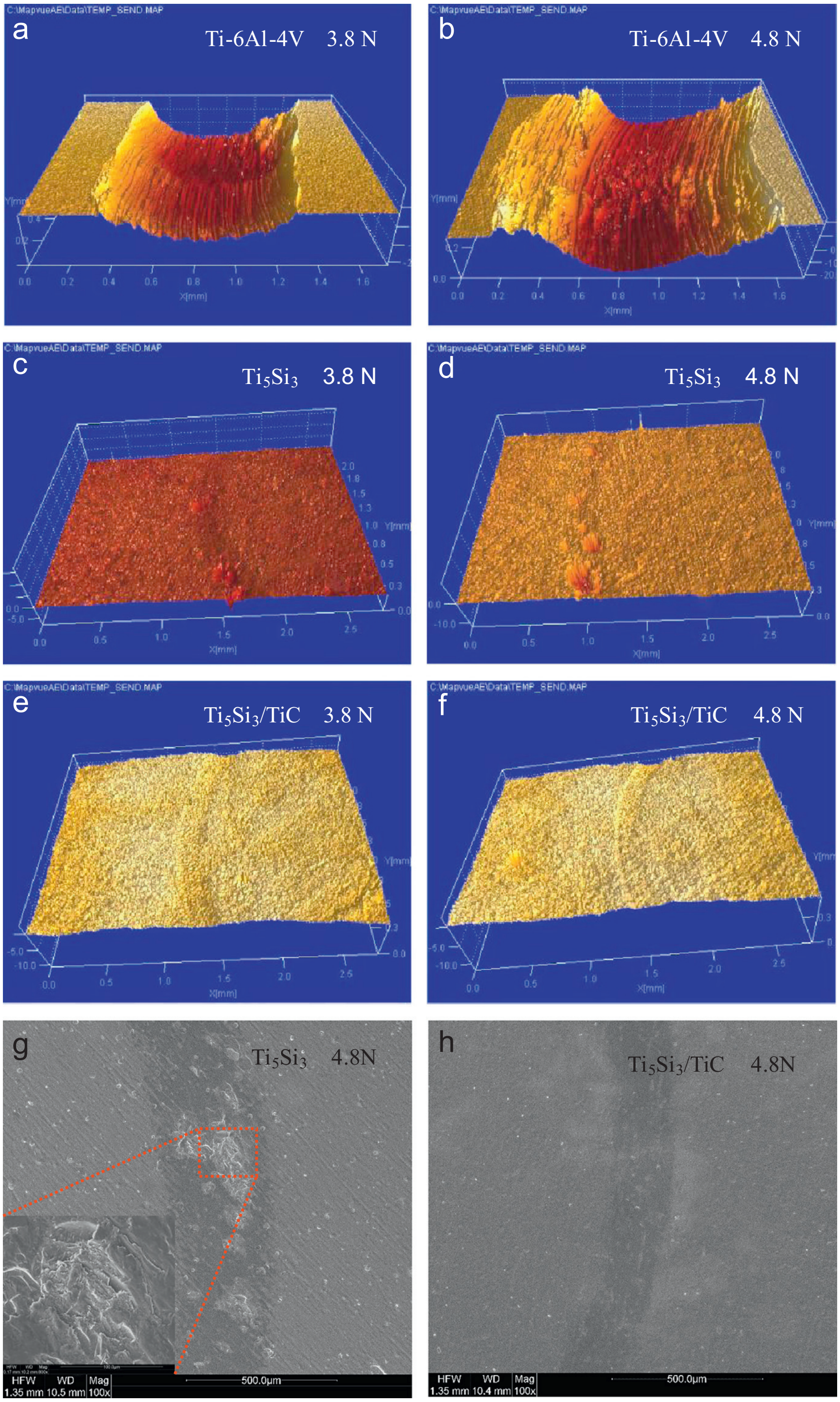

Fig. 9. Three-dimensional profiles of wear scars for the uncoated Ti–6Al–4V alloy and two as-deposited nanocrystalline coatings (a–f) and SEM micrographs of the worn surfaces of the Ti_5Si_3 nanocrystalline coating (g) and the Ti_5Si_3/TiC nanocomposite coating (h) as sliding against ZrO_2 ceramic ball under the normal loads of 4.8 N.

10 min and then reaches a quasi-steady-state value. With increasing applied normal load, the steady-state friction coefficients of the two as-deposited coatings and the uncoated Ti–6Al–4V substrate increase, and under each tested load, the steady-state friction coefficients of the two as-deposited coatings are reduced by 0.3–0.4 as compared to the uncoated Ti–6Al–4V substrate. This might be attributed to a decrease in the real contact area and alleviating surface plastic removal due to the higher surface hardness for the as-deposited coatings. Fig. 8 shows the specific wear rates of the two as-deposited coatings and the uncoated Ti–6Al–4V substrate. When the applied normal load increases from 3.8 N to 4.8 N, the specific wear rates of the uncoated Ti–6Al–4V substrate increase from 7.4×10^{-4} to $8.1\times10^{-4}\ \mathrm{mm^3\,N^{-1}\,m^{-1}}$, whereas the specific wear rates of the two as-deposited coatings are almost independent of the applied normal loads and are two orders of magnitude less than those of uncoated Ti–6Al–4V alloy, being around $10^{-6}\ \mathrm{mm^3\,N^{-1}\,m^{-1}}$. Under identical normal loads, the specific wear rates for the Ti_5Si_3/TiC nanocomposite coating are reduced by 30–40% as compared to the Ti_5Si_3 nanocrystalline coating, implying that wear resistance of a Ti_5Si_3 nanocrystalline coating is enhanced by the addition of TiC. It is worth noting that the specific wear rates are affected by the ratios of *H*/*E* for the two as-deposited coatings. In order to gain deeper insights into the wear mechanisms, the worn morphologies of the two as-deposited coatings and the uncoated Ti–6Al–4V substrate were analyzed using 3D profile measurements and SEM (Fig. 9). As seen in Fig. 9(a) and (b), the worn surfaces of untreated Ti–6Al–4V substrate display numerous deep and wide grooves along the sliding direction due to the surface deformation plowing by hard surface asperities of the ZrO_2 ceramic ball, together with some craters from adhesive detachment, suggesting that the dominant wear mechanisms of the uncoated Ti–6Al–4V substrate are severe abrasive and adhesive wear. At a higher normal load (4.8 N), the wear track of the Ti–6Al–4V becomes wider and deeper, which is also in agreement with a larger steady-state friction coefficient. In contrast, the two as-deposited coatings exhibit signs of very slight damage, characterized by a smooth worn surface with narrow and shallow plowing grooves. SEM inspection of the worn surfaces (Fig.9(g) and (h)) further indicates that there are some peeling micro-craters with some micro-cracks at the bottom of the worn track of the Ti_5Si_3 nanocrystalline coating, suggesting that brittle micro-fracture is predominant material removal mechanism for the monolithic Ti_5Si_3 nanocrystalline coating and leads to the higher specific wear rates in this coating with respect to the Ti_5Si_3/TiC nanocomposite coating. Previous studies have shown that for hard, brittle materials such as ceramics, the wear resistance is always proportional to $H^{1/2}K_{IC}^{3/4}$, indicating that fracture toughness is more important than the hardness for enhancing the wear resistance of brittle materials [44]. This may explain why the wear volume loss of these materials through brittle fracture processes is typically greater than that by plastic deformation processes [45].In terms of the above mechanical properties data, the addition of TiC to Ti_5Si_3 increases the load bearing capacity, hardness and fracture toughness of the Ti_5Si_3/TiC nanocomposite coating, and consequently has a positive effect on its wear behavior relative to the monolithic Ti_5Si_3 nanocrystalline coating, as evidenced by a shallow wear track without visible microcraters or spallation.

4. Conclusions

In summary, a novel Ti_5Si_3/TiC nanocomposite coating was prepared onto a Ti–6Al–4V substrate by a double cathode glow discharge in an attempt to improve its poor tribological properties. The Ti_5Si_3/TiC nanocomposite coating consists of cauliflower-like Ti_5Si_3 grains with TiC nanoparticles distributed at the grain boundaries. The mechanical and tribological properties of the Ti_5Si_3/TiC nanocomposite coating were characterized by nanoindentation, scratch, Vickers indentations and dry sliding wear tests. Compared to the monolithic Ti_5Si_3 nanocrystalline coating, the hardness, elastic strain to failure (*H*/*E*) and fracture toughness are significantly increased by the addition of TiC–Ti_5Si_3. Under dry sliding wear conditions, the specific wear rates of the Ti_5Si_3/TiC nanocomposite coating decrease by two orders of magnitude and 30–40%, respectively, as compared to the uncoated Ti–6Al–4V substrate and the monolithic Ti_5Si_3 nanocrystalline coating. The results show that an increase in the fracture toughness of the Ti_5Si_3/TiC nanocomposite coating, combined with higher hardness, has a positive effect on its wear behavior.

Acknowledgment

The authors acknowledge the financial support of the National Natural Science Foundation of China under grant no. 51175245 and the Technology Creative Project of Excellent Middle & Young Team of Hubei Province, China (grant no. T201207).

References

[1] F. Wang, Q.-L. Bi, X.-B. Wang, W.-M. Liu, Sliding friction and wear performance of Ti_6Al_4V in the presence of surface-capped copper nanoclusters lubricant, Tribology International 41 (3) (2008) 158–165.

[2] A. Tóth, M. Mohai, T. Ujvári, T. Bell, H. Dong, I. Bertóti, Surface chemical and nanomechanical aspects of air PIII-treated Ti and Ti-alloy, Surface and Coatings Technology 186 (1–2) (2004) 248–254.

[3] M. Qiu, Y.-Z. Zhang, S.G. Bao, S.-M. Du, Z.-W. Yan, The relationships between tribological behavior and heat-transfer capability of Ti_6Al_4V alloys, Wear 263 (1–6) (2007) 653–657.

[4] C.H. Hager Jr., J.H. Sandersb, S. Sharma, Unlubricated gross slip fretting wear of metallic plasma-sprayed coatings for Ti_6Al_4V surfaces, Wear 265 (3–4) (2008) 439–451.

[5] D.G. Bansal, O.L. Eryilmaz, P.J. Blau, Surface engineering to improve the durability and lubricity of Ti–6Al–4V alloy, Wear 271 (9–10) (2011) 2006–2015.

[6] Y. Wang, H.M. Wang, Wear resistance of laser clad Ti_2Ni_3Si reinforced intermetallic composite coatings on titanium alloy, Applied Surface Science 229 (1–4) (2004) 81–86.

[7] M.M. Silva, M. Ueda, L. Pichon, H. Reuther, C.M. Lepienski, Surface modification of Ti_6Al_4V alloy by PIII at high temperatures: effects of plasma potential, Nuclear Instruments and Materials in Physics Research B 257 (1–2) (2007) 722–726.

[8] K.-T. Rie, T. Stucky, R.A. Silva, E. Leitão, K. Bordji, J.-Y. Jouzeau, D. Mainard, Plasma surface treatment and PACVD on Ti alloys for

surgical implants, Surface and Coatings Technology 74–75 (2) (1995) 973–980.

[9] D.-H. Kuo, K.-W. Huang, Kinetics and microstructure of TiN coatings by CVD, Surface and Coatings Technology 135 (2–3) (2001) 150–157.

[10] B. Škorić, D. Kakaš, N. Bibic, M. Rakita, Microstructural studies of TiN coatings prepared by PVD and IBAD, Surface Science 566–568 (1) (2004) 40–44.

[11] T. Polcar, R. Novák, P. Široký, The tribological characteristics of TiCN coating at elevated temperatures, Wear 260 (1–2) (2006) 40–49.

[12] J. Xu, C.Z. Zhuo, J. Tao, S.Y. Jiang, The effect of second-phase on the corrosion and wear behaviors of composite alloying layer, Applied Surface Science 255 (5) (2008) 2688–2696.

[13] J. Xu, L.L. Liu, Z.-H. Xie, P. Munroe, Nanocomposite bilayer film for resisting wear and corrosion damage of a Ti–6Al–4V alloy, Surface and Coatings Technology 206 (19–20) (2012) 4156–4165.

[14] Z.H. Tang, J.J. Williams, A.J. Thom, M. Akinc, High temperature oxidation behavior of Ti_5Si_3-based intermetallics, Intermetallics 16 (9) (2008) 1118–1124.

[15] K. Kishida, M. Fujiwara, H. Adachi, K. Tanaka, H. Inui, Plastic deformation of single crystals of Ti_5Si_3 with the hexagonal D88 structure, Acta Materialia 58 (3) (2010) 846–857.

[16] C.L. Yeh, W.H. Chen, C.C. Hsu, Formation of titanium silicides Ti_5Si_3 and $TiSi_2$ by self-propagating combustion synthesis, Journal of Alloys and Compounds 432 (1–2) (2007) 90–95.

[17] M.H. Enayati, F. Karimzadeh, S.Z. Anvari, Synthesis of nanocrystalline NiAl by mechanical alloying, Journal of Materials Processing Technology 200 (1–3) (2008) 312–315.

[18] J.L. Li, D.L. Jiang, S.H. Tan, Microstructure and mechanical properties of in situ produced Ti_5Si_3/TiC nanocomposites, Journal of the European Ceramic Society 22 (4) (2002) 551–558.

[19] R. Mitra, Microstructure and mechanical behavior of reaction hot-pressed titanium silicide and titanium silicide-based alloys and composites, Metallurgical and Materials Transaction A 29 (6) (1998) 1629–1641.

[20] L.J. Wang, W. Jiang, C. Qin, L.D. Chen, In-situ synthesized Ti_5Si_3/TiC composites by spark plasma sintering technology, Journal of Materials Science 41 (12) (2006) 3831–3835.

[21] J. Xu, Y. Wang, S.Y. Jiang, The effect of substitution of Cr for Mo on the mechanical properties of nanocrystalline Mo_5Si_3 films, Nanoscale 2 (3) (2010) 394–398.

[22] W.C. Oliver, G.M. Pharr, An improved technique for determining hardness and elastic modulus using load and displacement sensing indentation experiments, Journal of Materials Research 7 (6) (1992) 1564–1583.

[23] J. Xu, L.L. Liu, X.L. Lu, S.Y. Jiang, Effect of carbon doping on electrochemical behavior of nanocrystalline Ti_5Si_3 film in NaCl solution, Electrochemistry Communications 13 (1) (2011) 102–105.

[24] L. Zhang, J. Wu, Ti_5Si_3 and Ti_5Si_3-based alloys: Alloying behavior, microstructure and mechanical property evaluation, Acta Materialia 46 (10) (1998) 3535–3546.

[25] J. Xu, X.Z. Mao, Z.-H. Xie, P. Munroe, Damage-tolerant, hard nanocomposite coatings enabled by a hierarchical structure, Journal of Physical Chemistry C 115 (39) (2011) 18977–18982.

[26] C.A. Schuh, T.G. Nieh, H. Iwasaki, The effect of solid solution W additions on the mechanical properties of nanocrystalline Ni, Acta Materialia 51 (2) (2003) 431–443.

[27] V. Yamakov, D. Wolf, S.R. Phillpot, A.K. Mukherjee, H. Gleiter, Deformation-mechanism map for nanocrystalline metals by molecular-dynamic simulation, Nature Materials 3 (2004) 43–47.

[28] Z.W. Shan, E.A. Stach, J.M.K. Wiezorek, J.A. Knapp, D.M. Follstaedt, S.X. Mao, Grain boundary-mediated plasticity in nanocrystalline nickel, Science 305 (5684) (2004) 654–657.

[29] F.M. Gao, J.L. He, E.D. Wu, S.M. Liu, D.L. Yu, D.C. Li, S.Y. Zhang, Y.J. Tian, Hardness of covalent crystals, Physical Review Letters 91 (1) (2003) 015502.

[30] J.S. Tse, D.D. Klug, F.M. Gao, Hardness of nanocrystalline diamonds, Physical Review B 73 (14) (2006) 140102.

[31] A. Leyland, A. Matthews, On the significance of the H/E ratio in wear control: a nanocomposite coating approach to optimized tribological behavior, Wear 246 (1-2) (2000) 1–11.

[32] S.-K. Bae, I.-J. Shon, J.-M. Doh, J.-K. Yoon, I.-Y. Ko, Properties and consolidation of nanocrystalline $NbSi_2$–SiC–Si_3N_4 composite by pulsed current activated combustion, Scripta Materialia 58 (6) (2008) 425–428.

[33] J.H. Schneibel, C.J. Rawn, E.A. Payzant, C.L. Fu, Controlling the thermal expansion anisotropy of Mo_5Si_3 and Ti_5Si_3 silicides, Intermetallics 12 (7–9) (2004) 845–850.

[34] L.T. Zhang, J.S. Wu, Thermal expansion and elastic moduli of the silicide based intermetallic alloys $Ti_5Si_3(X)$ and Nb_5Si_3, Scripta Materialia 38 (2) (1998) 307–313.

[35] S. Reuss, H. Vehoff, Temperature dependence of the fracture toughness of single phase and two phase intermetallics, Scripta Metallurgica et Materialia 24 (6) (1990) 1021–1026.

[36] D.M. Shah, D. Berczik, D.L. Anton, R. Hecht, Appraisal of other silicides as structural materials, Materials Science and Engineering: A 155 (1–2) (1992) 45–57.

[37] A.J. Thom, M.K. Meyer, Y. Kim, M. Akinc, in: V.A. Ravi, T.S. Srivatsan, J.J. Moore (Eds.), Processing and fabrication of advanced materials III, TMS, Warrendale, USA, 1994, p. 413.

[38] C.L. Fu, X.D. Wang, Thermal expansion coefficient of Mo–Si compounds by first-principles calculations, Philosophical Magazine Letters 80 (10) (2000) 683–690.

[39] J.J. Williams, M.J. Kramer, M. Akinc, Thermal expansion of Ti_5Si_3 with Ge, B, C, N, or O additions, Journal of Materials Research 15 (8) (2000) 1780–1785.

[40] S. Hogmark, S. Jacobson, M. Larsson, Design and evaluation of tribological coatings, Wear 246 (1–2) (2000) 20–33.

[41] X. Ma, A. Matthews, Investigation of abradable seal coating performance using scratch testing, Surface and Coatings Technology 202 (4–7) (2007) 1214–1220.

[42] Z. Chen, L.Y.L. Wu, E. Chwa, O. Tham, Scratch resistance of brittle thin films on compliant substrates, Materials Science and Engineering: A 493 (1–2) (2008) 292–298.

[43] Z.X. Zhang, H. Dong, T. Bell, The load bearing capacity of hydrogen-free Cr-DLC coatings on deep-case oxygen hardened Ti_6Al_4V, Surface and Coatings Technology 200 (18–19) (2006) 5237–5244.

[44] P.S. Tantri, E.M. Jayasingh, S.K. Biswas, S.K. Ramasesha, Role of in situ generated tribofilm on the tribological characteristics of monolith and TiB_2 reinforced $MoSi_2$ intermetallic, Materials Science and Engineering: A 336 (1–2) (2002) 64–71.

[45] B.R. Lawn, A.G. Evans, D.B. Marshall, Elastic/plastic indentation damage in ceramics: The median/radial crack system, Journal of the American Ceramic Society 63 (9–10) (1980) 574–581.